PCCP

ROYAL SOCIETY OF CHEMISTRY

PAPER

View Article Online
View Journal | View Issue

Cite this: *Phys. Chem. Chem. Phys.*, 2026, **28**, 7331

Identifying the active nickel sites and hydrogen species in the phosphosulfide overlayer on the Ni_2P hydrotreating catalyst: a DFT-D3 study

Alba B. Vidal, *[a] José Luis Peña-Mena,[a] Rafael Añez,[a] David S. Coll,[b] Oscar Hurtado-Aular,[c] Aníbal Sierraalta [a] and Joaquin L. Brito [de]

Received 20th January 2026,
Accepted 26th February 2026

DOI: 10.1039/d6cp00205f

rsc.li/pccp

Density functional theory (DFT) calculations and an atomistic thermodynamic approach were employed to identify the active nickel sites and determine the chemical nature of the hydrogen species in the nickel phosphosulfide overlayer formed on the (0001) and (10$\bar{1}$0) surfaces of the Ni_2P hydrotreating catalyst. Our results showed that Ni(1) sites are less resistant to sulfur than Ni(2) sites, in agreement with experimental observations. Under HDS conditions, the fully sulfided (0001) surface of Ni_2P was found to be structurally similar to the (111) surface of the low-activity sulfide Ni_3S_2, where closely coordinated Ni atoms are prone to sulfidation. Non-hydrogenated surfaces were always the most stable, suggesting that NiH and SH groups are unlikely to form on these surfaces. In contrast, the most stable (10$\bar{1}$0) surface was identified as a hydrogenated surface with coordinatively unsaturated Ni(2) atoms surrounded by SH groups. Depending on the electronegativity of their ligands (S or Ni), the hydrogen species exhibit either protonic ($H^{\delta+}$) or hydridic ($H^{\delta-}$) character. Our results suggest that protons within SH groups are the most likely reactive hydrogen species on the nickel phosphosulfide overlayer under reaction conditions, providing atomic-level insight into the origins of HYD activity in Ni_2P catalysts.

1. Introduction

Nickel phosphide (Ni_2P) has emerged as a promising candidate for a new generation of industrial hydrodesulfurization (HDS) catalysts.[1–7] According to the literature, the active phase of the Ni_2P catalyst is a nickel phosphosulfide overlayer that forms during the HDS reaction.[1,8–12] This overlayer can also be generated by pretreatment with sulfidation agents, such as H_2S or CS_2 in the presence of H_2, or by reducing sulfur-containing precursors, such as nickel hexathiodiphosphate ($Ni_2P_2S_6$).[13–16]

The active sites in HDS catalysts are primarily linked to coordinatively unsaturated metal sites (CUSs), sulfhydryl (SH) groups, and metal hydrides (MH).[17,18] CUSs are S^{2-} anion vacancies located at the edges or corners of catalyst nanoparticles. SH groups, on the other hand, result from the dissociative adsorption of H_2 onto surface sulfur atoms. These groups behave as Brønsted acid sites.[19,20] MH species are formed when H_2 dissociatively adsorbs onto CUSs. Consequently, it is essential to understand the structural changes of Ni_2P under reaction conditions and the specific catalytic functions of the active sites.

In an early study, Oyama *et al.* investigated the catalytic activity of Ni_2P supported on low- and high-surface-area siliceous supports (SiO_2-L, SiO_2-H, and MCM-41) for the HDS of 4,6-dimethyldibenzothiophene (4,6-DMDBT).[21] Extended X-ray absorption fine structure (EXAFS) analysis confirmed the presence of two types of nickel sites: Ni(1), with tetrahedral coordination to P, and Ni(2), with square pyramidal coordination to P. The analysis further revealed both Ni(1) and Ni(2) sites are present in large crystallites, whereas Ni(2) sites are more numerous on the small crystallites. Catalytic selectivity measurements showed that small crystallites exhibit higher selectivity toward HYD products, while large crystallites have higher selectivity toward DDS products. Based on product selectivity, it was concluded that the Ni(1) sites are primarily responsible for the DDS pathway, while the Ni(2) sites are highly active for the HYD pathway.

In a later study, Oyama *et al.* investigated the sulfur-resistant properties of the Ni_2P catalyst in deep hydrodesulfurization.[3] EXAFS analysis of spent catalysts revealed that Ni(2) sites are

[a] *Laboratorio de Química Física y Catálisis Computacional, Centro de Química "Dr Gabriel Chuchani", Instituto Venezolano de Investigaciones Científicas (IVIC), Apartado 21827, Caracas, Venezuela. E-mail: abvidals@gmail.com*
[b] *Laboratorio de Físico Química Teórica de Materiales, Centro de Química "Dr Gabriel Chuchani", Instituto Venezolano de Investigaciones Científicas (IVIC), Apartado 21827, Caracas, Venezuela*
[c] *Departamento de Química, Universidad Nacional del Sur (UNS), Av. Alem 1253, Bahía Blanca, 8000, Argentina*
[d] *Laboratorio de Físico Química de Superficies, Centro de Química "Dr Gabriel Chuchani", Instituto Venezolano de Investigaciones Científicas (IVIC), Apartado 21827, Caracas, Venezuela*
[e] *Biomass to Resources Group, Universidad Regional Amazónica IKIAM, Tena, Ecuador*

bound to sulfur with a lower Ni–S coordination as the particle size decreased. Based on EXAFS results, the authors concluded that the active Ni(2) sites on highly dispersed Ni_2P catalysts are much more tolerant of sulfur than the tetrahedral Ni(1) sites. Furthermore, the higher selectivity for HYD products correlates with an increased number of surface Ni(2) sites, which predominate in smaller Ni_2P particles.

To elucidate the catalytic mechanism of the HDS reaction on the Ni_2P catalyst, it is essential to understand the state of adsorbed hydrogen on the nickel phosphosulfide overlayer. To the best of our knowledge, there are no experimental studies on the chemical nature of hydrogen species adsorbed on Ni_2P as an HDS catalyst. Only Nelson *et al.*, using density functional theory (DFT) calculations, have studied the presence of SH groups on the (0001) surface of the Ni_2P catalyst.[22] The authors calculated the free energy changes associated with H_2S adsorption and its dissociation into –SH and sulfur on the (0001) Ni_3P_2-terminated surface as a function of temperature (100–1000 K) under H_2 and H_2S partial pressures of 5.0 and 0.1 MPa, respectively. Their results indicated that the relative stability of the adsorbed sulfur species follows the order $H_2S < SH < S$. These results suggest that hydrogen bound as an SH group might not be thermodynamically stable under HDS reaction conditions.

On the other hand, electrocatalysis experiments have shown that incorporating sulfur improves the performance of Ni_2P in the hydrogen evolution reaction (HER).[23–25] Although the HER and HDS occur under different conditions, both processes involve hydrogen atoms adsorbed on the surface.[26] It was found that sulfur incorporation accelerates the adsorption rate of reaction intermediates on the catalyst surface, thereby improving HER kinetics. Therefore, sulfur incorporated into the catalyst may act as an activity promoter or selectivity modifier.[27]

In this work, we combined DFT calculations with an atomistic thermodynamic analysis to investigate the stability of hydrogen species on the phosphosulfide overlayer formed on the (0001) and (10$\bar{1}$0) surfaces of the Ni_2P catalyst under HDS conditions. Our goal is to elucidate the nature of the active nickel sites and the chemical characteristics of the hydrogen species, which are key to understanding the hydrogenation functionality of the phosphosulfide overlayer.

2. Computational details

2.1. Computational methods

DFT calculations were performed using the Vienna *ab initio* simulation package (VASP).[28,29] The Perdew–Burke–Ernzerhof exchange–correlation functional with a generalized gradient approximation was used.[30] The projector augmented wave (PAW) method was used to describe the electron–ion interactions.[31] Standard PAW potentials with a valence electron distribution of Ni $3d^84s^2$, P $3s^23p^3$, S $3s^23p^4$, and H $1s^1$ were used. A plane-wave kinetic energy cut-off of 400 eV was employed. The energy and atomic force convergence criteria were set to 10^{-5} eV and 0.01 eV $Å^{-1}$, respectively. The Gaussian smearing method with a width of 0.05 eV was used to describe the partial occupancies of the electronic states. The DFT-D3 correction developed by Grimme *et al.* was used to capture dispersion interactions, which are important to the energetics of catalytic transformations.[32–35] Gamma-centered *k*-point meshes of $5 \times 5 \times 9$ and $7 \times 7 \times 7$ were used to sample the Brillouin zone for the optimization of bulk Ni_2P and Ni_3S_2, respectively. The calculated lattice parameters for bulk Ni_2P are $a = b = 5.836$ Å and $c = 3.307$ Å, while for bulk Ni_3S_2 (rhombohedral representation), $a = b = c = 4.034$ Å. These values are in good agreement with the reported experimental values for Ni_2P ($a = b = 5.859$ Å, $c = 3.382$ Å)[36] and Ni_3S_2 ($a = b = c = 4.082$ Å).[37] All surface calculations were performed using symmetric slabs. The (0001) Ni_3P_2 surface termination was modeled using a nine-atomic-layer (2×2) slab with a $3 \times 3 \times 1$ gamma-centered *k*-point mesh (Fig. S1a). The (10$\bar{1}$0) AB Ni_2P surface termination was modeled with ten-atomic-layer (2×2) slabs with a $3 \times 5 \times 1$ Monkhorst–Pack *k*-point mesh (Fig. S1b). The (111) surface of Ni_3S_2 was modeled with eight-atomic-layer (2×2) slab with a $3 \times 3 \times 1$ gamma-centered *k*-point mesh (Fig. S1c). A vacuum space of 20 Å was set to avoid interactions between periodic slabs, and all atoms were fully relaxed during the calculations. Bader charge[38] and electron density difference (EDD) analyses were performed to assess the charge distribution and the chemical nature of the hydrogen species adsorbed on the surface. The EDD was calculated from the following equation:

$$\Delta\rho = \rho(\text{surface + adsorbate}) - \rho(\text{surface}) - \rho(\text{adsorbate}) \quad (1)$$

where ρ(surface + adsorbate) is the electron density of the whole system, ρ(surface) and ρ(adsorbate) are the electron densities of the surface, and the adsorbate calculated at the adsorption positions, respectively. The VESTA program was used to visualize the electron density difference isosurfaces.[39]

2.2. Surface models

To construct slab models of the possible structures of the nickel phosphosulfide overlayer on the Ni_2P catalyst, we selected the (0001) and (10$\bar{1}$0) surfaces. Papawassiliou *et al.*,[40] using ^{31}P solid-state nuclear magnetic resonance (ssNMR), high-resolution transmission electron microscopy (HRTEM), X-ray diffraction (XRD), and DFT calculations, determined that Ni_2P nanoparticles synthesized under excess phosphorus predominantly expose these surfaces. For the (0001) surface, the slab model was constructed from a (2×2) supercell with a Ni_3P_2 termination. This surface termination has been reported as the most thermodynamically stable.[41,42] The surface is described by a hexagonal supercell ($a = b = 11.672$ Å) and contains eight P atoms and twelve Ni atoms in the outermost atomic layer, $Ni_{12}P_8$ (Fig. S1a). These Ni atoms are referred to as Ni(1). On the surface, the Ni(1) atoms form four three-fold adsorption sites (Ni_3 sites), which are labeled as T sites, as illustrated in Fig. S1. For the (10$\bar{1}$0) surface, the slab model surface was constructed from a (2×2) supercell with the AB-type Ni_2P termination, which has also been reported as the most thermodynamically stable surface termination.[41,42] The surface is described by a rectangular supercell (a = 11.672 Å and

b = 6.614 Å) and contains four P atoms and eight Ni atoms in the outermost atomic layer, Ni_8P_4 (Fig. S1b). This surface contains two distinct types of Ni atoms: four Ni(1) and Ni(2). In Fig. S1b the Ni(2) nickel atoms are represented by light blue spheres to distinguish them from the Ni(1) nickel atoms. On the surface, the Ni atoms adopt a zigzag arrangement along the y-axis. (Fig. S1). This zigzag configuration exhibits two types of Ni_3 sites: four T1 sites and four T2 sites. Each T1 site consists of two Ni(1) atoms and one Ni(2) atom, while the T2 site consists of two Ni(2) atoms and one Ni(1) atom. It has been shown that the S atoms are preferentially located at the T1 sites.[42] At 50%S, the S atoms are preferentially adsorbed at the T1 sites in an alternating configuration. The adsorption energy difference between T1 and T2 sites was around 1 eV. For the (111) surface of the Ni_3S_2 catalyst (rhombohedral representation), the slab model was constructed from a (2 × 2) supercell with the Ni_3S_2 termination. The surface is described by a hexagonal supercell ($a = b$ = 11.360 Å), with eight S atoms and twelve Ni atoms in the outermost atomic layer, $Ni_{12}S_8$ (Fig. S1c). The surface Ni atoms also form four Ni_3 sites, which are also labeled as T sites.

The slab models of the nickel phosphosulfide overlayer on the $(10\bar{1}0)$ and (0001) surfaces were constructed following the surface modification procedure previously reported.[42] These slab models take into account the processes of sulfur adsorption and the replacement of surface phosphorus by sulfur at the outermost atomic layer. For the (0001)-$Ni_{12}P_8$ surface, the replacement of P by S was evaluated at 0%, 50%, and 100% of S, where 0%S corresponds to no replacement, 50%S corresponds to replacement with four S atoms, and 100%S corresponds to replacement with eight S atoms. Additionally, sulfur adsorption was evaluated at coverages of 75%S and 100%S, which correspond to the adsorption of three and four S atoms, respectively. Surface terminations are labeled according to the elemental composition of the outermost layer and the number of S atoms adsorbed. For the $(10\bar{1}0)$-Ni_8P_4 surface, the replacement of P by S was evaluated at 0%, 50%, and 100% of S, where 0%S corresponds to no replacement, 50%S corresponds to replacement with two S atoms, and 100%S corresponds to replacement with four S atoms. This surface has two types of adsorption sites for sulfur: four T1 sites and four T2 sites (Fig. S1b). For the slab models of the hydrogenated surfaces, we evaluated the dissociative adsorption of one or two H_2 molecules, corresponding to hydrogen coverages of 50% and 100%, respectively.

2.3. Thermodynamic approach

Since HDS operating conditions are sulforeductive conditions in which H_2 is more abundant than H_2S in the gas phase, PH_3 could be produced when P atoms are replaced by S atoms in the presence of H_2. Therefore, the possibility of complete sulfidation of bulk Ni_2P to bulk Ni_3S_2 under relevant conditions was evaluated by the following reaction:

$$Ni_2P(bulk) + 4/3H_2S + 3/2H_2 \rightarrow 2/3Ni_3S_2(bulk) + PH_3 + 4/3H_2 \quad (2)$$

and the corresponding Gibbs free energy, $\left(\Delta G_{\text{Sulfidation}}^{Ni_2P\rightarrow Ni_3S_2}\right)$, is then given by

$$\Delta G_{\text{Sulfidation}}^{Ni_2P\rightarrow Ni_3S_2}(T,p) = (2/3)E_{Ni_3S_2}^{\text{bulk}} - E_{Ni_2P}^{\text{bulk}} + \mu_P(T,p) - (4/3)\mu_S(T,p) \quad (3)$$

where $E_{Ni_3S_2}^{\text{bulk}}$ and $E_{Ni_2P}^{\text{bulk}}$ are the DFT total energies of bulk Ni_3S_2 and Ni_2P phases, respectively. The chemical potential of phosphorus, $\mu_P(T, p)$, is determined by the chemical equilibrium with the gas-phase mixture of PH_3 and H_2,

$$\mu_P(T,p) = \mu_{PH_3}(T,p) - (3/2)\mu_{H_2}(T,p) \quad (4)$$

$\mu_{PH_3}(T, p)$ and $\mu_{H_2}(T, p)$ are the chemical potentials of PH_3 and H_2, respectively, evaluated assuming ideal gas behavior. The calculations of chemical potentials are more detailed in the SI.

On the other hand, the chemical potential of sulfur, $\mu_S(T, p)$, is determined by the chemical equilibrium with the gas-phase mixture of H_2 and H_2S,

$$\mu_S(T,p) = \mu_{H_2S}(T,p) - \mu_{H_2}(T,p) \quad (5)$$

where $\mu_{H_2S}(T, p)$ and $\mu_{H_2}(T, p)$ are the chemical potentials of H_2S and H_2, respectively, also evaluated assuming ideal gas behavior. Under typical HDS conditions, the $\frac{p_{H_2S}}{p_{H_2}}$ ratio ranges from 0.01 to 0.05, and the temperature varies between 573 and 700 K. In this study, we selected 573 K as the working temperature because several experimental studies using Ni_2P catalyst have performed HDS measurements at this temperature.[1,2,10,12,13]

The possibility of replacing the surface P atoms with S atoms, as well as the adsorption of S atoms under relevant conditions, can be described as

$$Ni_xP_y + (z+a)H_2S + (3/2z)H_2 \rightarrow Ni_xP_{(y-z)}S_{z-a}S + zPH_3 + (z+a)H_2 \quad (6)$$

The Gibbs free energy associated with these processes (adsorption and replacement) can be calculated as follows:

$$\Delta G(T,p) = E_{Ni_xP_{(y-z)}S_{z-a}S}^{\text{slab}} - E_{Ni_xP_y}^{\text{slab}} + z\mu_P(T,p) - (z+a)\mu_S(T,p) \quad (7)$$

where $E_{Ni_xP_{(y-z)}S_{z-a}S}^{\text{slab}}$ is the DFT total energy of a slab model (either the (0001). or $(10\bar{1}0)$ surface), in which z surface phosphorus atoms have been replaced by sulfur atoms, in addition to the adsorption of a sulfur atoms on the Ni_3 sites. $E_{Ni_xP_y}^{\text{slab}}$ is the DFT total energy of the pristine surface, which is taken as a reference.

On the other hand, the Gibbs free energy change associated only with S atom adsorption ($\Delta G_{\text{ads}}^{S}$), is given by

$$\Delta G_{\text{ads}}^{S} = E_{Ni_xP_{(y-z)}S_{z-a}S}^{\text{slab}} - E_{Ni_xP_{(y-z)}S_z}^{\text{slab}} - a\mu_S(T,p) \quad (8)$$

where $E_{Ni_xP_{(y-z)}S_z}^{\text{slab}}$ and $E_{Ni_xP_{(y-z)}S_{z-a}S}^{\text{slab}}$ are the DFT total energy of sulfided and clean surfaces, respectively. a is the number of S atoms adsorbed.

Finally, the dissociative adsorption of H_2 as NiH or SH groups on the nickel phosphosulfide overlayer was evaluated by the following reaction:

$$Ni_xP_{(y-z)}S_z\_aS + nH_2 \rightarrow Ni_xP_{(y-z)}S_z\_aS\_2nH \quad (9)$$

and the corresponding Gibbs free energy, $\left(\Delta G^{H_2}_{diss}\right)$, is given by

$$\Delta G^{H_2}_{diss} = E^{slab}_{Ni_xP_{(y-z)}S_z\_aS\_2nH} - E^{slab}_{Ni_xP_{(y-z)}S_z\_aS} - 2n\mu_H(T,p) \quad (10)$$

where $E^{slab}_{Ni_xP_{(y-z)}S_z\_aS\_2nH}$ and $E^{slab}_{Ni_xP_{(y-z)}S_z\_aS}$ are the DFT total energy of hydrogenated and non-hydrogenated surfaces, respectively. n is the number of dissociatively adsorbed H_2 molecules, and $\mu_H(T,p)$ is the hydrogen chemical potential, where $\mu_H(T,p) = (\frac{1}{2})\mu_{H_2}(T,p)$.

3. Results and discussion

3.1. Bulk Ni_2P stability under the H_2S/H_2 gas mixture

Group 8 transition metal catalysts (nickel, palladium, and platinum) are highly susceptible to sulfur poisoning, with nickel being the most susceptible to sulfide formation.[43–45] However, nickel phosphide-based catalysts have been shown to be highly resistant to sulfur poisoning.[3,7,12,46] Given that Ni_3S_2 is the most stable stoichiometry of nickel sulfide under HDS reaction conditions,[47–49] we investigated the relative stability of bulk Ni_2P over bulk Ni_3S_2 in the presence of the H_2S/H_2 gas mixture. Bulk Ni_2P belongs to the hexagonal crystal system with the $P\bar{6}2m$ space group (Fig. 1a). It is characterized by the presence of two distinct types of Ni atoms, denoted as Ni(1) and Ni(2).[21,50] Ni(1) atoms have a quasi-tetrahedral coordination

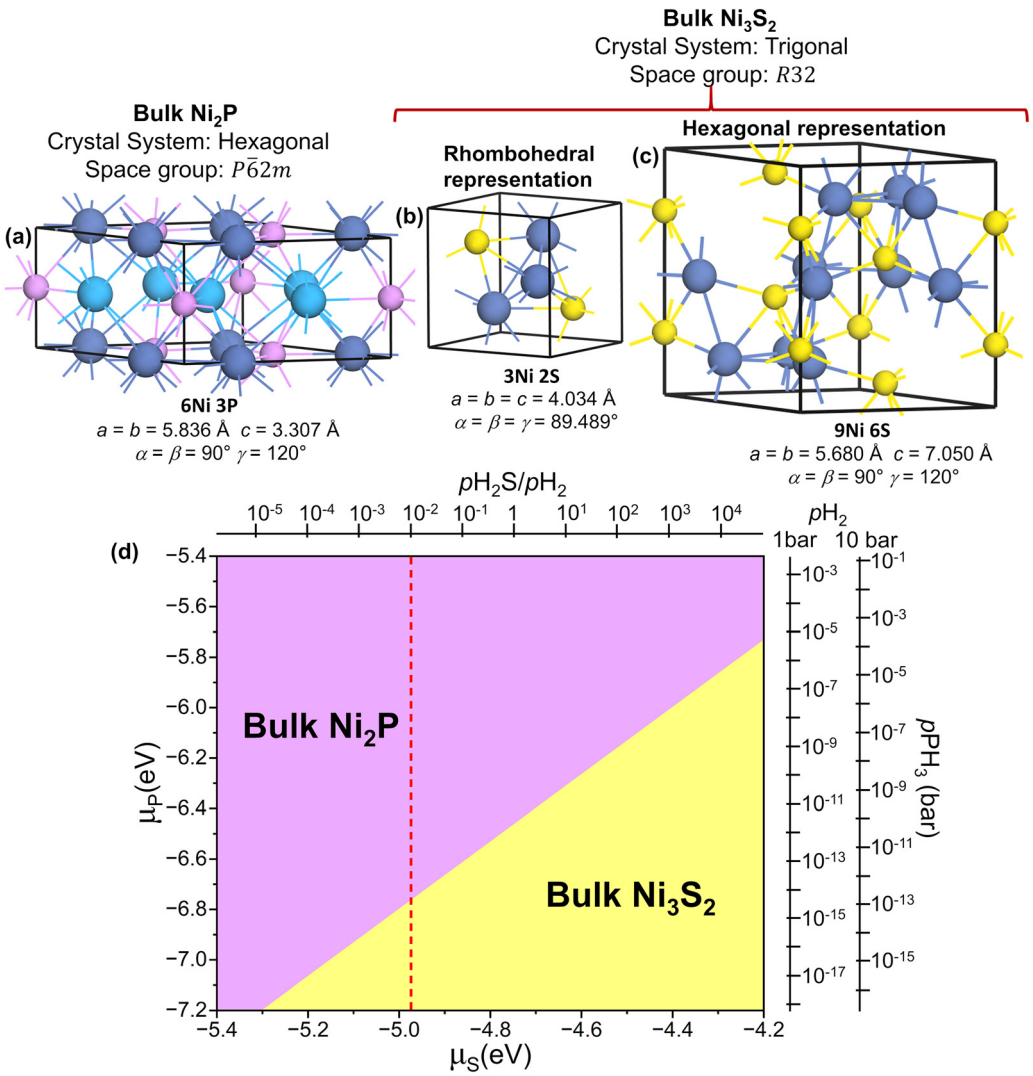

Fig. 1 Optimized crystal structure of (a) bulk Ni_2P, (b) bulk Ni_3S_2 in the rhombohedral representation, and (c) bulk Ni_3S_2 in the hexagonal representation. Blue, light blue, pink, and yellow spheres are the Ni(1) nickel, Ni(2) nickel, phosphorus, and sulfur atoms, respectively. (d) Phase diagram for the complete sulfidation of bulk Ni_2P to bulk Ni_3S_2 as a function of $\mu_P(T,p)$ and $\mu_S(T,p)$. The dependence of the chemical potentials with the gas phase is translated into pressure scales for T = 573 K on the upper x-axis for the H_2S/H_2 mixture and on the right y-axis for PH_3 at p_{H_2} = 1 and 10 bar. The red dotted line corresponds to typical HDS partial pressures ratio, $\frac{p_{H_2S}}{p_{H_2}} = 0.01$.

geometry with the four nearest-neighbor P atoms, while Ni(2) atoms exhibit a square pyramidal coordination geometry with the five nearest-neighbor P atoms. In Fig. 1a the Ni(2) nickel atoms are represented by light blue spheres to distinguish them from the Ni(1) nickel atoms. Bulk Ni_3S_2 belongs to the trigonal crystal system with the *R*32 space group. It can be described in both rhombohedral (Fig. 1b) and hexagonal (Fig. 1c) lattice representations. This bulk only has one type of Ni atom, which has a quasi-tetrahedral coordination geometry with the four nearest-neighbor S atoms.

Fig. 1d shows the phase diagram of the free energy change for complete sulfidation of bulk Ni_2P to bulk Ni_3S_2 as a function of $\mu_P(T, p)$ and $\mu_S(T, p)$. The regions of stability of the bulk phases are represented by the distinct colored areas. The red dotted line in Fig. 1d represents a typical HDS $\frac{p_{H_2S}}{p_{H_2}}$ ratio. It is observed that the complete sulfidation of Ni_2P to Ni_3S_2 may occur when $\mu_P(T, p)$ is lower than −6.77 eV. At 573 K, this condition is met when p_{PH_3} is lower than 3×10^{-15} bar with p_{H_2} = 1 bar or when p_{PH_3} is lower than 10^{-13} bar with p_{H_2} = 10 bar. PH_3 is a very strong phosphiding agent, and consequently, competition could exist between the sulfidation and phosphidation processes. Our findings suggest that bulk Ni_2P will not undergo complete sulfidation to bulk Ni_3S_2 as long as there is a trace amount of PH_3 in the gas phase. This result correlates with the sulfur resistance observed in Ni_2P catalysts under HDS conditions.[3,7,12,46]

3.2. Phosphosulfide overlayer on the (0001) surface

We revisited the adsorption and replacement processes of sulfur atoms on the (0001) surface by calculating the free energy change as a function of the phosphorus and sulfur chemical potentials, $\mu_P(T, p)$ and $\mu_S(T, p)$. The analysis was carried out considering the thermodynamic limit in which bulk Ni_2P transforms into bulk Ni_3S_2. Fig. 2a presents the corresponding free energy phase diagram. The stability regions of the different surface compositions are indicated by the different shades of green. Fig. 2b–d show the top view of the corresponding surface structures. Surface terminations are labeled according to the elemental composition of the outermost layer and the number of S atoms adsorbed. In Fig. 2a, the red dotted line represents a typical HDS $\frac{p_{H_2S}}{p_{H_2}}$ ratio, while the blue dotted line indicates the phase boundary between the bulk Ni_2P and Ni_3S_2. The (0001)-$Ni_{12}P_8$_4S, (0001)-$Ni_{12}P_4S_4$_4S, and (0001)-$Ni_{12}S_8$_4S surfaces are the most stable at a $\frac{p_{H_2S}}{p_{H_2}}$ ratio of 0.01. All of these surfaces have all Ni_3 sites covered by S atoms. The findings of this study are consistent with those previously reported.[42]

Note that the (0001)-$Ni_{12}S_8$_4S surface is the most stable at very low PH_3 partial pressures. In the context of HDS experiments, the presence of PH_3 in the gas mixture has not been detected, suggesting that only a trace amount of PH_3 might be produced by the replacement of surface P atoms by S atoms. In contrast to the bulk phase, a very low p_{PH_3} enables the gradual replacement of all surface P atoms with S atoms, resulting in

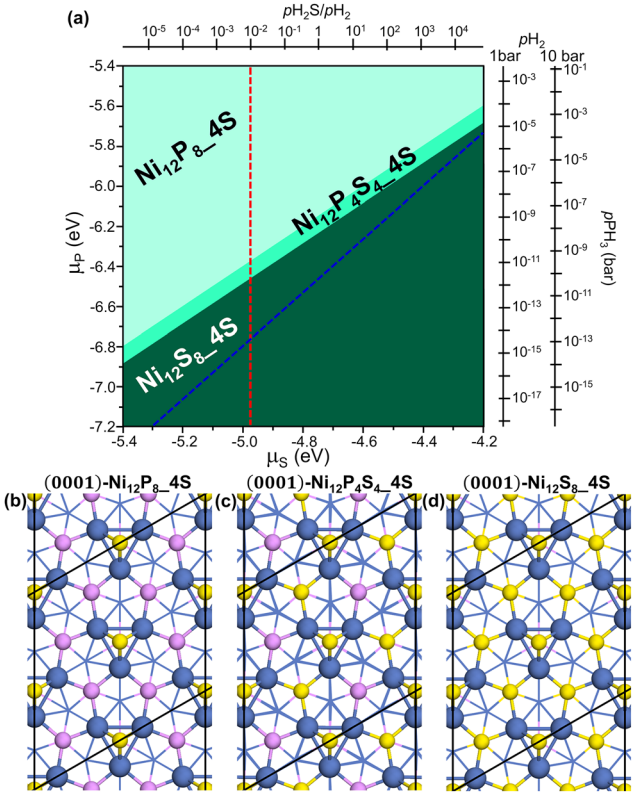

Fig. 2 (a) Phase diagram of the most stable (0001)-$Ni_xP_{y-z}S_z$_$S_{z'}$ surface composition as a function of $\mu_P(T, p)$ and $\mu_S(T, p)$. The dependence of the chemical potentials with the gas phase is translated into pressure scales for T = 573 K on the upper *x*-axis for the H_2S/H_2 mixture and on the right *y*-axis for PH_3 at p_{H_2} = 1 and 10 bar. The red dotted line corresponds to the typical HDS partial pressure ratio, $\frac{p_{H_2S}}{p_{H_2}} = 0.01$. The blue dotted line indicates the phase boundary between the bulk Ni_2P and Ni_3S_2. Top view of the optimized structures of the (2 × 2) supercell: (b) (0001)-$Ni_{12}P_8$_4S, (c) (0001)-$Ni_{12}P_4S_4$_4S, and (d) (0001)-$Ni_{12}S_8$_4S surfaces. Blue, pink, and yellow spheres are the nickel, phosphorus, and sulfur atoms, respectively.

the formation of a phosphosulfide overlayer on the (0001)-$Ni_{12}P_8$ surface termination. Therefore, our results suggest that the (0001)-$Ni_{12}S_8$_4S surface could be the most stable surface termination under HDS reaction conditions. In this regard, Oyama *et al.* used EXAFS technique to study the structural properties of supported Ni_2P catalysts after the HDS reaction of 4,6-dimethyldibenzothiophene.[3] According to EXAFS line shape analysis, catalysts with shorter Ni–Ni bond lengths are more likely to form a phosphosulfide phase. It was found that the tetrahedral Ni(1) sites are less resistant to sulfur than the square-pyramidal Ni(2) sites. On the (0001) surface, the Ni(1) atoms are closely coordinated with another two Ni(1) atoms and, therefore, may be prone to sulfidation. For the Ni_2P catalyst, the active sites are believed to be the coordinatively unsaturated surface nickel atoms belonging to the phosphosulfide phase. Our results suggest that the (0001)-$Ni_{12}S_8$_4S surface could not be active under HDS conditions because the Ni_3 sites, which consist of Ni(1)-type atoms, would be blocked by sulfur atoms.

It is noteworthy that the surface structure of the (0001)-$Ni_{12}S_8$_4S surface of Ni_2P closely resembles that of the (111)-$Ni_{12}S_8$_4S surface of Ni_3S_2 (Fig. 3a and b). Both surface terminations share the same composition and feature Ni_3 sites, where each Ni atom is bonded to two surface S atoms. The Ni–Ni bond distances are 2.646 Å and 2.558 Å, respectively. On the (0001)-$Ni_{12}S_8$_4S surface, the Ni_3 sites are capped above by an S atom and below a P atom. On the (111)-$Ni_{12}S_8$_4S surface, the Ni_3 sites are capped above and below by an S atom. This results in an almost regular trigonal bipyramid. It is well known that Ni_3S_2 catalysts exhibit very low activity in various hydrotreating reactions.[47,48,51] In this regard, Aray *et al.* used DFT calculations to investigate the surface stability of the low-index Miller surfaces and the equilibrium morphology of the Ni_3S_2 catalyst.[52] It was found that only the (111) and (11$\bar{1}$) type surface faces are exposed under HDS conditions. The S-covered surfaces were the most stable in the whole range of the $\frac{p_{H_2S}}{p_{H_2}}$ ratio. These findings suggested that the surfaces of the Ni_3S_2 catalyst may not have coordinatively unsaturated metal sites available for the reaction.

For comparison, we calculated the Gibbs free energy change associated with S atoms adsorption (ΔG^{S}_{ads}) on the (0001)-$Ni_{12}S_8$ and the (111)-$Ni_{12}S_8$ surfaces as a function of $\mu_S(T, p)$ (Fig. 3c and d). The clean surface was taken as a reference. Additionally, ΔG^{S}_{ads} was calculated for the (0001)-$Ni_{12}P_8$ and (0001)-$Ni_{12}P_4S_4$ surfaces (Fig. S2). It is observed that the fully covered surfaces (with four S atoms adsorbed) are the most stable across the entire range of evaluated $\mu_S(T, p)$. For example, at T = 573 K and $\frac{p_{H_2S}}{p_{H_2}} = 0.01$, the energy required to create a sulfur vacancy on the fully covered surface shows the following trend: (111)-$Ni_{12}S_8$_4S (1.06 eV) ≈ (0001)-$Ni_{12}P_8$_4S (1.05 eV) > (0001)-$Ni_{12}P_4S_4$_4S (0.63 eV) > (0001)-$Ni_{12}S_8$_4S (0.46 eV). For the (0001) surface, vacancy formation becomes energetically more favorable as surface P atoms are replaced by S atoms; this is due to the strain effect exerted by the S atoms.[42] Within our thermodynamic framework, surfaces with coordinatively unsaturated sites consisting of spatially isolated Ni_3 ensembles may not be stable under HDS conditions.

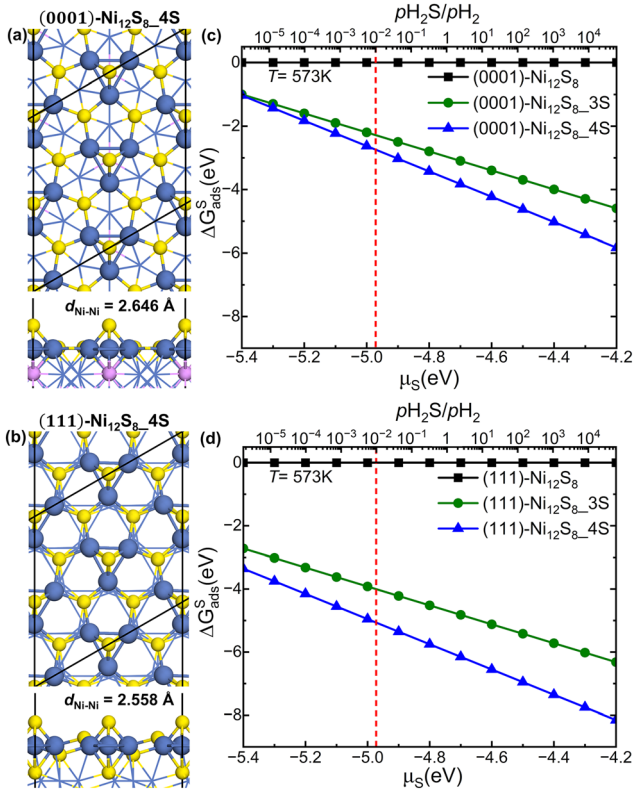

Fig. 3 Top and side views of the optimized structures of the (2 × 2) supercell: (a) (0001)-$Ni_{12}S_8$_4S and (b) (111)-$Ni_{12}S_8$_4S surfaces. Blue, pink, and yellow spheres are the nickel, phosphorus, and sulfur atoms, respectively. (c) and (d) ΔG^{S}_{ads} as a function of $\mu_S(T, p)$, respectively. The dependence of $\mu_S(T, p)$ with the gas phase H_2S/H_2 mixture is translated into pressure scales for T = 573 K. The red dotted line corresponds to the typical HDS partial pressure ratio, $\frac{p_{H_2S}}{p_{H_2}} = 0.01$. The clean surfaces are taken as a reference.

3.3. Dissociative adsorption of H_2 onto the phosphosulfide overlayer on the (0001) surface

Dissociative adsorption of H_2 onto the nickel phosphosulfide overlayer can lead to the formation of SH or NiH groups. Fig. 4a–d show the optimized structures of the hydrogenated surfaces resulting from the dissociative adsorption of one and two H_2 molecules on the (0001)-$Ni_{12}S_8$_4S and (111)-$Ni_{12}S_8$_4S surfaces. Fig. S3 shows the configurations evaluated for the dissociative adsorption of one H_2 molecule on the (0001)-$Ni_{12}S_8$_4S surface. When the SH group forms, the sulfur atom binds to two of the three Ni(1) atoms at the Ni_3 site. This leaves the third Ni(1) atom coordinatively unsaturated. Fig. 4e and f display $\Delta G^{H_2}_{diss}$ as a function of $\mu_H(T, p)$. The non-hydrogenated surface was taken as a reference. We also calculated $\Delta G^{H_2}_{diss}$ for the (0001)-$Ni_{12}P_8$_4S and (0001)-$Ni_{12}P_4S_4$_4S surfaces (Fig. S4). The configurations evaluated for the dissociative adsorption of one H_2 molecule on the (0001)-$Ni_{12}P_8$_4S and (0001)-$Ni_{12}P_4S_4$_4S surfaces are shown in Fig. S5 and S6, respectively. It is observed that the weakest hydrogen adsorption occurs on the (111)-$Ni_{12}S_8$_4S surface. For example, at T = 573 K and p_{H_2} = 10 bar, the energy required for the dissociative adsorption of one H_2 molecule shows the following trend: (111)-$Ni_{12}S_8$_2S_2SH (0.97 eV) > (0001)-$Ni_{12}P_8$_2S_2SH (0.68 eV) > (0001)-$Ni_{12}P_4S_4$_2S_2SH (0.62 eV) > (0001)-$Ni_{12}S_8$_2S_2SH (0.39 eV). For the dissociative adsorption of two H_2 molecules on fully sulfur-covered surfaces, the corresponding energy trend is: (111)-$Ni_{12}S_8$_4SH (1.94 eV) > (0001)-$Ni_{12}P_8$_4SH (1.44 eV) > (0001)-$Ni_{12}P_4S_4$_4SH (1.34 eV) > (0001)-$Ni_{12}S_8$_4SH (1.05 eV). For the (0001) surface, hydrogen dissociative adsorption surface becomes energetically favorable as surface P atoms are replaced by S atoms. Nevertheless, non-hydrogenated surfaces are always the most stable, which suggests that SH groups are unlikely to form on these surfaces.

3.4. Phosphosulfide overlayer on the (10$\bar{1}$0) surface

Fig. 5a shows the phase diagram of the free energy change for the processes of adsorption and replacement by S atoms on the (10$\bar{1}$0) surface as a function of $\mu_P(T, p)$ and $\mu_S(T, p)$. The stability

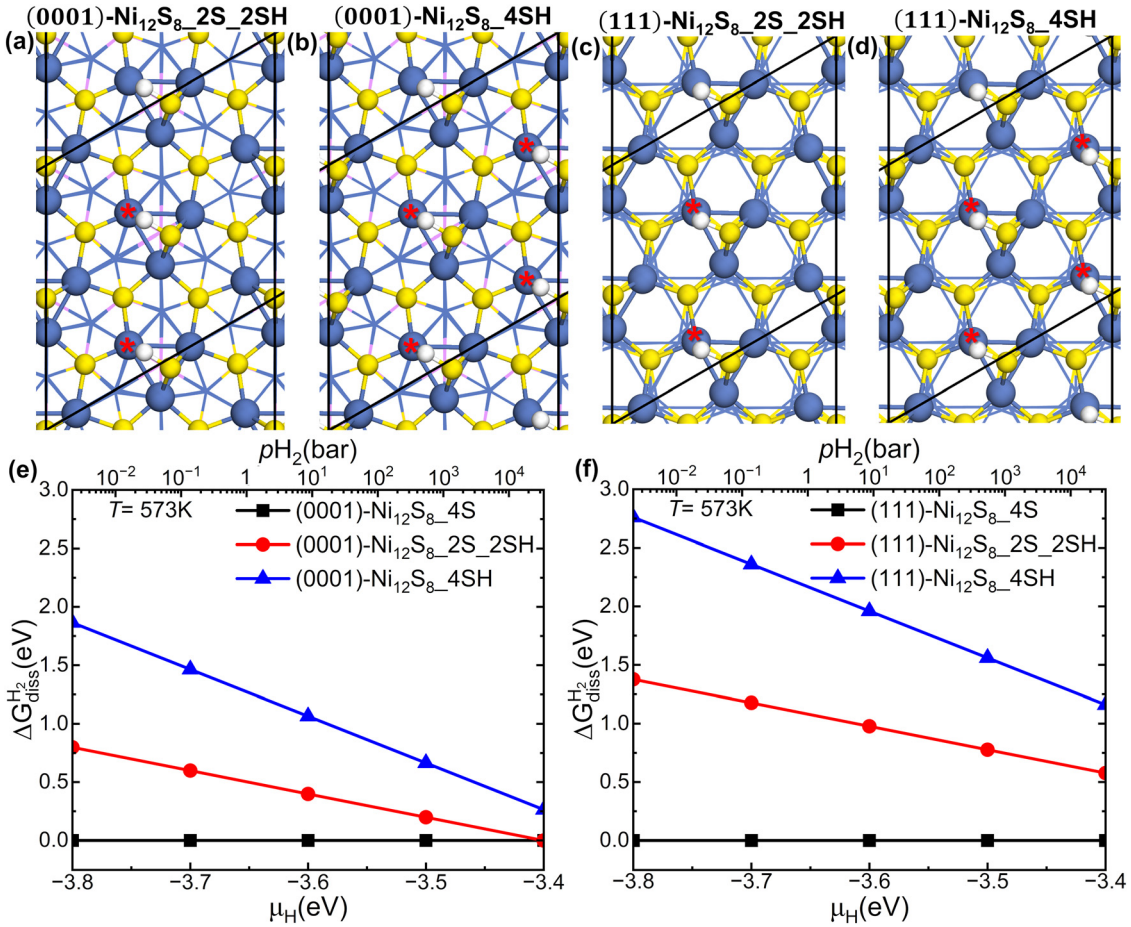

Fig. 4 Top view of the optimized structures of the (2 × 2) supercell of hydrogenated surfaces: (a) (0001)-$Ni_{12}S_8$_2S_2SH, (b) (0001)-$Ni_{12}S_8$_4SH, (c) (111)-$Ni_{12}S_8$_2S_2SH, and (d) (111)-$Ni_{12}S_8$_4SH. Blue, yellow, and white spheres are the nickel, sulfur, and hydrogen atoms, respectively. (e) and (f) $\Delta G_{diss}^{H_2}$ as a function of $\mu_H(T, p)$, respectively. The dependence of $\mu_H(T, p)$ with the gas phase H_2 is translated into pressure scales for T = 573 K. The non-hydrogenated surface was taken as a reference. Coordinatively unsaturated nickel atoms are marked by a red asterisk.

regions of the different surface compositions are indicated by the different shades of green. Fig. 5b–g show the top views of the corresponding surface structures. In all of these surfaces, S atoms are preferentially adsorbed at the T1 sites. In Fig. 6a, the red dotted line represents a typical HDS $\frac{p_{H_2S}}{p_{H_2}}$ ratio, while the blue dotted line indicates the phase boundary between the bulk Ni_2P and Ni_3S_2. The $(10\bar{1}0)$-Ni_8P_4_2S, $(10\bar{1}0)$-$Ni_8P_2S_2$_2S, and $(10\bar{1}0)$-Ni_8S_4_2S surfaces are the most stable at a $\frac{p_{H_2S}}{p_{H_2}}$ ratio of 0.01. All of these surfaces have the Ni_3 sites partially covered by S atoms in an alternating configuration. The findings of this study are consistent with those previously reported.[42] It is observed that the $(10\bar{1}0)$-Ni_8S_4_2S surface is the most stable at very low PH_3 partial pressures. Therefore, our results suggest that the $(10\bar{1}0)$-Ni_8S_4_2S surface could be the most stable surface termination under HDS reaction conditions. On the $(10\bar{1}0)$-Ni_8S_4_2S surface, each T1 site consists of two Ni(1) atoms and one Ni(2) atom, with the Ni(1) atoms shared with the next T1 site. As a result, on the uncovered T1 sites, only the Ni(2) atoms are coordinatively unsaturated (Fig. 5f). Our findings are consistent with the EXAFS results by Oyama *et al.* that showed the square-pyramidal Ni(2) sites bind to sulfur with a lower Ni-S coordination.[3] Therefore, the nickel phosphosulfide phase contains coordinatively unsaturated Ni(2)-type atoms available for the HDS reaction.

3.5. Dissociative adsorption of H_2 onto the phosphosulfide overlayer on the $(10\bar{1}0)$ surface

Fig. 6a shows the phase diagram of the free energy change for the dissociative adsorption of one and two H_2 molecules on the $(10\bar{1}0)$-Ni_8S_4_2S and $(10\bar{1}0)$-Ni_8S_4_4S surfaces as a function of $\mu_H(T, p)$ and $\mu_S(T, p)$. The $(10\bar{1}0)$-Ni_8S_4_2S surface is taken as a reference. For example, the dissociative adsorption of two H_2 molecules in the $(10\bar{1}0)$-Ni_8S_4_4S surface was calculated as $\Delta G_{diss}^{H_2} = E_{Ni_8S_4\_4SH}^{slab} - E_{Ni_8S_4\_2S}^{slab} - 4\mu_H(T,p) - 2\mu_S(T,p)$. Fig. 6b–d show the optimized structures for the most stable hydrogenated surfaces. Fig. S7 shows the configurations evaluated for the dissociative adsorption of one H_2 molecule on the $(10\bar{1}0)$-Ni_8S_4_2S. When H adsorbs to form an SH group, the S atom binds in a bridging position between the Ni(1) and Ni(2) atoms.

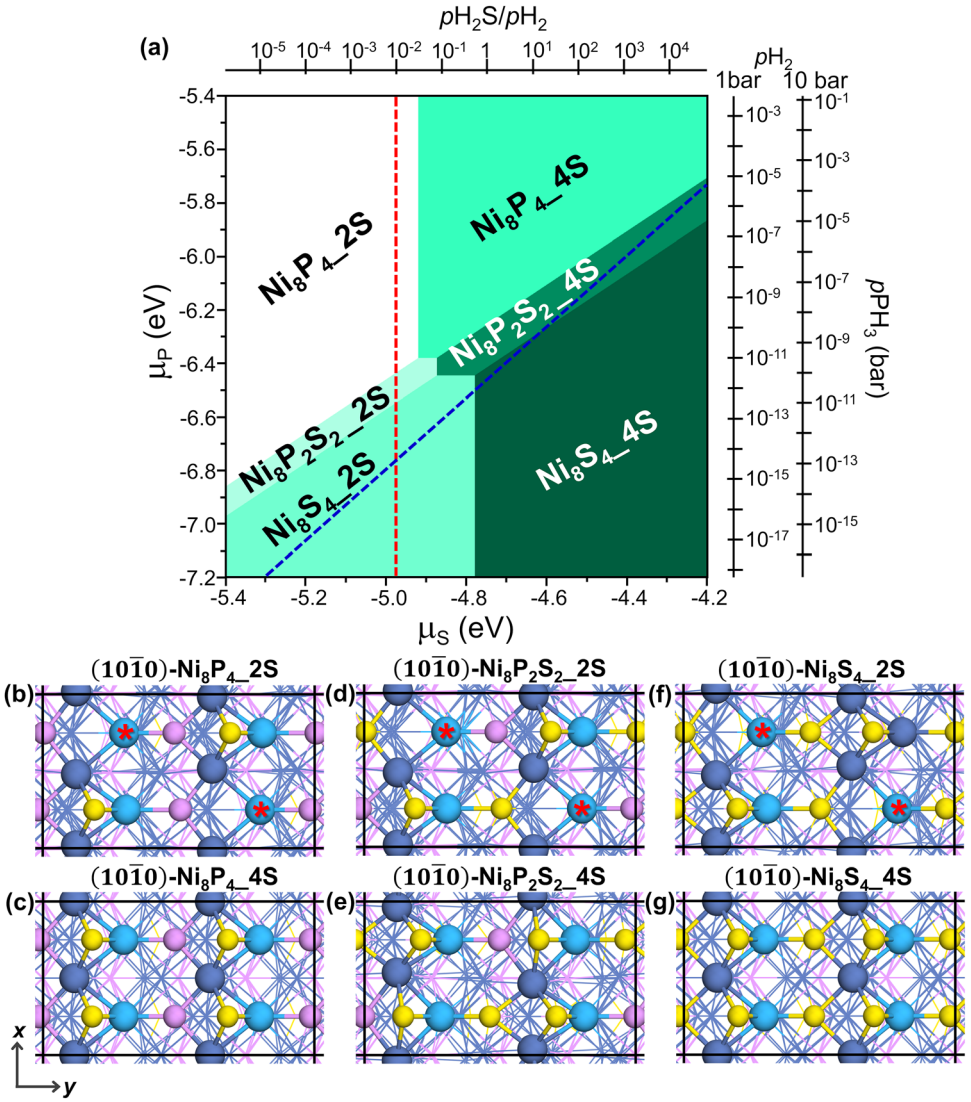

Fig. 5 (a) Phase diagram of the most stable (10$\bar{1}$0)-$Ni_xP_{y-z}S_z$_$S_{z'}$ surface composition as a function of $\mu_P(T, p)$ and $\mu_S(T, p)$. The dependence of the chemical potentials with the gas phase is translated into pressure scales for T = 573 K on the upper x-axis for the H_2S/H_2 mixture and on the right y-axis for PH_3 at p_{H_2} = 1 and 10 bar. The red dotted line corresponds to the typical HDS partial pressure ratio, $\frac{p_{H_2S}}{p_{H_2}} = 0.01$. The blue dotted line indicates the phase boundary between the bulk Ni_2P and Ni_3S_2. Top view of the optimized structures of the (2 × 2) supercell: (b) (10$\bar{1}$0)-Ni_8P_4_2S, (c) (10$\bar{1}$0)-Ni_8P_4_4S, (d) (10$\bar{1}$0)-$Ni_8P_2S_2$_2S, (e) (10$\bar{1}$0)-$Ni_8P_2S_2$_4S, (f) (10$\bar{1}$0)-Ni_8S_4_2S, and (g) (10$\bar{1}$0)-Ni_8S_4_4S surfaces. Blue, light blue, pink, and yellow spheres are the Ni(1) nickel, Ni(2) nickel, phosphorus, and sulfur atoms, respectively. Coordinatively unsaturated Ni(2) nickel atoms are marked by a red asterisk.

Similarly, when the H atom adsorbs to form a NiH species, it occupies a bridging position between the Ni(1) and Ni(2) atoms. For the (10$\bar{1}$0)-Ni_8S_4_2S surface, the dissociative adsorption of one H_2 molecule produces two SH groups, leading to the (10$\bar{1}$0)-Ni_8S_4_2SH surface (Fig. 6b). When the SH groups form on this surface, two Ni(1) atoms become coordinatively unsaturated. On the other hand, the dissociative adsorption of two H_2 molecules produces two SH groups and two NiH groups, leading to the (10$\bar{1}$0)-Ni_8S_4_2SH_2NiH surface (Fig. 6c). For the (10$\bar{1}$0)-Ni_8S_4_4S surface, the dissociative adsorption of two H_2 molecules produces four SH groups, leading to the (10$\bar{1}$0)-Ni_8S_4_4SH surface (Fig. 6d). We also calculated the phase diagram of the free energy change for the dissociative adsorption of H_2 on the (10$\bar{1}$0)-Ni_8P_4_2S, (10$\bar{1}$0)-Ni_8P_4_4S, (10$\bar{1}$0)-$Ni_8P_2S_2$_2S, and (10$\bar{1}$0)-$Ni_8P_2S_2$_4S surfaces (Fig. S8). The configurations evaluated for the dissociative adsorption of one H_2 molecule on the (10$\bar{1}$0)-Ni_8P_4_2S and (10$\bar{1}$0)-$Ni_8P_2S_2$_2S surfaces are shown in Fig. S9 and S10, respectively.

As shown in Fig. 6a, keeping the $\frac{p_{H_2S}}{p_{H_2}}$ ratio constant at 0.01 while increasing p_{H_2}, results in two phase transitions at the most stable surface. First, the (10$\bar{1}$0)-Ni_8S_4_2S surface appears, and then the (10$\bar{1}$0)-Ni_8S_4_4SH surface. The hydrogenated surface (10$\bar{1}$0)-Ni_8S_4_4SH is stable at p_{H_2} above 10 bar. Hydrogenated surfaces resulting from the dissociative adsorption of H_2 on the (10$\bar{1}$0)-Ni_8S_4_2S surface become stable at lower $\frac{p_{H_2S}}{p_{H_2}}$

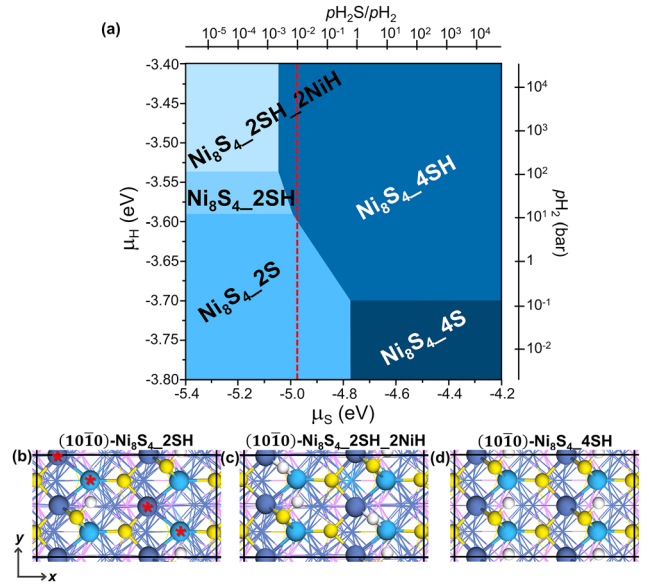

Fig. 6 (a) Phase diagram of the most stable hydrogenated surface composition for the (10$\bar{1}$0)-Ni_8S_4_2S and (10$\bar{1}$0)-Ni_8S_4_4S surfaces as a function of $\mu_H(T, p)$ and $\mu_S(T, p)$. The dependence of the chemical potentials with the gas phase is translated into pressure scales for T = 573 K on the upper x-axis for the H_2S/H_2 mixture and on the right y-axis for H_2. The red dotted line corresponds to the typical HDS partial pressure ratio, $\frac{p_{H_2S}}{p_{H_2}} = 0.01$. Top view of the optimized structures of the (2 × 2) supercell: (b) (10$\bar{1}$0)-Ni_8S_4_2SH, (c) (10$\bar{1}$0)-Ni_8S_4_2SH_2NiH, and (d) (10$\bar{1}$0)-Ni_8S_4_4SH hydrogenated surfaces. Blue, light blue, yellow, and white spheres are the Ni(1) nickel, Ni(2) nickel, sulfur, and hydrogen atoms, respectively. Coordinatively unsaturated Ni(1) and Ni(2) nickel atoms are marked by a red asterisk.

ratios and higher p_{H_2}. For instance, the (10$\bar{1}$0)-Ni_8S_4_2SH surface is stable at p_{H_2} above 10 bar, while the (10$\bar{1}$0)-Ni_8S_4_2SH_2NiH surface is stable at p_{H_2} above 100 bar. These results imply that surfaces with coordinatively unsaturated Ni(1) atoms, or with H atoms adsorbed in a bridging position between the Ni(1) and Ni(2) atoms, may only be stable under strong reducing conditions. This trend was also observed on the surfaces with 0% and 50% of replacement with S (Fig. S8). On the other hand, the energy required for the dissociative adsorption of two H_2 molecules on fully sulfur-covered surfaces at T = 573 K and p_{H_2} = 10 bar follows the trend: (10$\bar{1}$0)-Ni_8P_4_4SH (−0.07 eV) > (10$\bar{1}$0)-$Ni_8P_2S_2$_4SH (−0.14 eV) > (10$\bar{1}$0)-Ni_8S_4_4SH (−0.42 eV). These results suggest that replacing surface phosphorus atoms with sulfur promotes the H_2 dissociation process.

As mentioned above, Oyama *et al.* attribute the high HYD activity observed in small particles to the presence of S-resistant Ni(2) sites.[3] Therefore, we used a (2 × 4) supercell to explore the stability of surfaces with SH groups and coordinatively unsaturated Ni(2) atoms. The (2 × 4) supercell size is an expansion along the y-axis. We evaluated the dissociative adsorption of one, two, and four H_2 molecules, corresponding to hydrogen coverages of 25%, 50%, and 100%, respectively. The surface compositions evaluated were the (10$\bar{1}$0)-$Ni_{16}S_8$_4S, (10$\bar{1}$0)-$Ni_{16}S_8$_6S, and (10$\bar{1}$0)-$Ni_{16}S_8$_8S surfaces, which correspond to sulfur coverages of 50%, 75%, and 100%, respectively. The supercell models are shown in Fig. S11. Fig. 7a shows that the (10$\bar{1}$0)-$Ni_{16}S_8$_2S_4SH and (10$\bar{1}$0)-$Ni_{16}S_8$_6SH_2NiH surfaces are the most stable hydrogenated surfaces at a $\frac{p_{H_2S}}{p_{H_2}}$ ratio of 0.01. The (10$\bar{1}$0)-$Ni_{16}S_8$_6SH_2NiH surface is only stable at p_{H_2} above 10^4 bar. Additionally, it is found that the (10$\bar{1}$0)-$Ni_{16}S_8$_4SH surface, which has coordinatively unsaturated Ni(1) atoms, is not stable under any reaction conditions (Fig. S12). Surfaces with H atoms adsorbed in a bridging position between the Ni(1) and Ni(2) atoms, such as the (10$\bar{1}$0)-$Ni_{16}S_8$_4SH_4NiH surface, are only stable under strong reducing conditions. At high $\frac{p_{H_2S}}{p_{H_2}}$ ratios, the (10$\bar{1}$0)-$Ni_{16}S_8$_8SH surface is the most stable hydrogenated surface. These results suggest that hydrogenated surfaces, such as (10$\bar{1}$0)-$Ni_{16}S_8$_2S_4SH, which have coordinatively unsaturated Ni(2) atoms, may be stable under HDS reaction conditions. Note that the SH groups surround the Ni(2) atoms (Fig. 7b). These findings may help explain the high HYD selectivity observed at Ni(2) sites, as reported by Oyama *et al.*[3] Organosulfur compounds adsorbed on Ni(2) sites could react with H atoms from adjacent SH groups, which may result in the formation of hydrogenated intermediates and subsequent C–S bond cleavage. A detailed kinetic analysis of the HDS reaction mechanism, however, is beyond the scope of the present work.

To gain insight into the chemical nature of the hydrogen species on the surface, we performed Bader charge and electron density difference analyses. The formal charges of the different adsorbed species on the surface are H^-, SH^-, and S^{2-} The stabilization of hydrogen as a proton involves an oxidation process, as it is accompanied by the oxidation of S atoms within the SH group. In contrast, the stabilization of hydrogen as a hydride corresponds to a reduction process.[53] The Bader charges (q) of the surface atoms for the (10$\bar{1}$0)-$Ni_{16}S_8$_6S, (10$\bar{1}$0)-$Ni_{16}S_8$_2S_4SH and (10$\bar{1}$0)-$Ni_{16}S_8$_6SH_2NiH surfaces are summarized in Table 1. The hydrogen atoms are characterized by a different Bader charge, which reflects their chemical identities. For the (10$\bar{1}$0)-$Ni_{16}S_8$_2S_4SH surface, when H adsorbs as a proton (H^+) to form SH groups, each H atom carries a low positive charge of +0.04e. The charge on the S atoms is found to be more negative as S anions (−0.48e) than as SH groups (−0.30e). For the (10$\bar{1}$0)-$Ni_{16}S_8$_6SH_2NiH surface, when H adsorbs as a hydride (H^-), each H atom carries a negative charge of −0.17e. Cai *et al.* reported the Bader charge analysis of hydrogen atoms adsorbed on the RuS_2 catalyst. They found that hydrogen atoms bonded to sulfur atoms carry a positive charge ranging from +0.02e to +0.15e, whereas those adsorbed on ruthenium atoms exhibit a negative charge of approximately −0.20e.[18] The Bader charges obtained in our study are consistent with their results in terms of both magnitude and sign. We also calculated the EDD to illustrate the redistribution of electron density due to the interaction between these species and the surface. Fig. 8a and b show the EDD plots for the (10$\bar{1}$0)-$Ni_{16}S_8$_2S_4SH and (10$\bar{1}$0)-$Ni_{16}S_8$_6SH_2NiH surfaces, respectively. The densities of the S, H, and SH species were used as adsorbate references. In

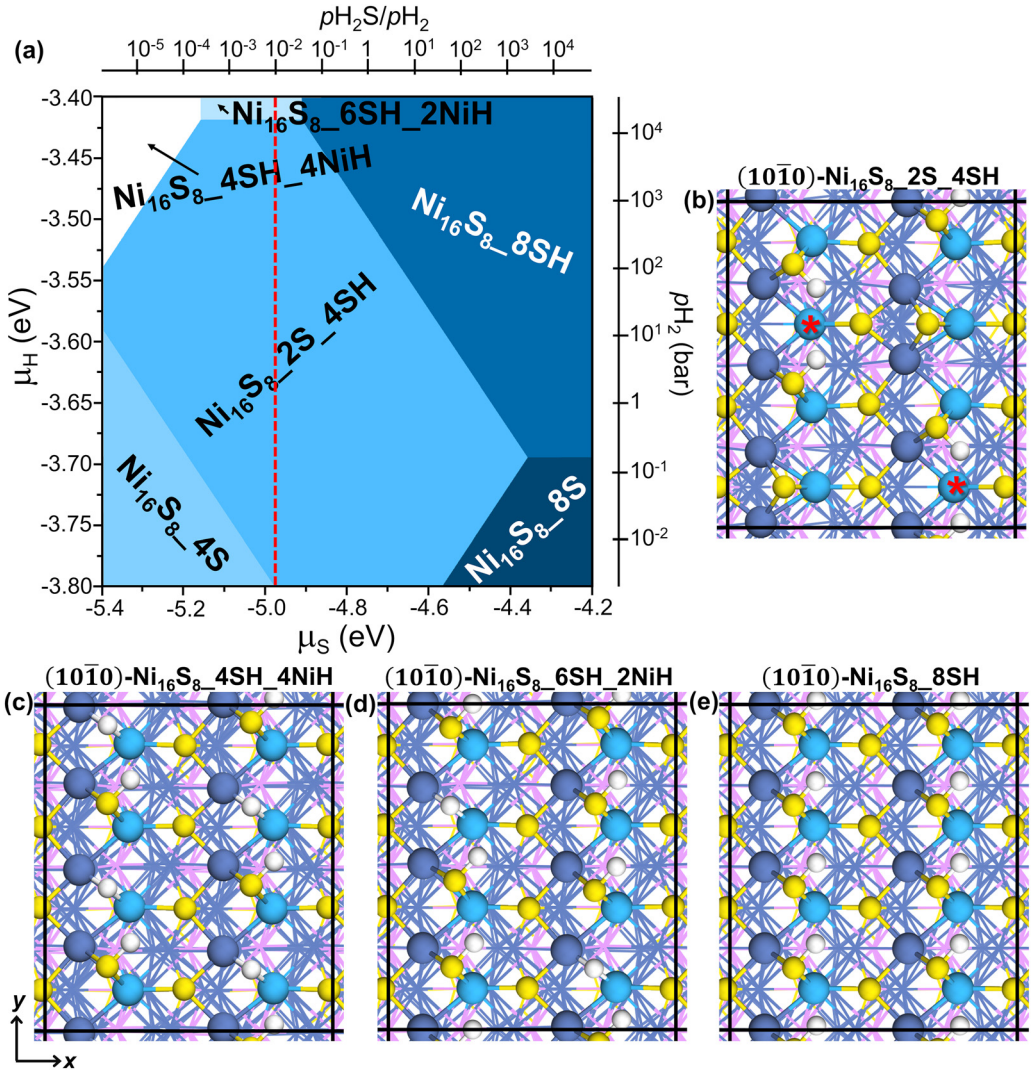

Fig. 7 (a) Phase diagram of the most stable hydrogenated surface composition for the $(10\bar{1}0)$-$Ni_{16}S_8$_4S, $(10\bar{1}0)$-$Ni_{16}S_8$_6S, and $(10\bar{1}0)$-$Ni_{16}S_8$_8S surfaces as a function of $\mu_H(T, p)$ and $\mu_S(T, p)$. The dependence of the chemical potentials with the gas phase is translated into pressure scales for T = 573 K on the upper x-axis for the H_2S/H_2 mixture and on the right y-axis for H_2. The red dotted line corresponds to the typical HDS partial pressure ratio, $\frac{p_{H_2S}}{p_{H_2}} = 0.01$. Top view of the optimized structures of the (2 × 4) supercell of the hydrogenated surfaces: (b) $(10\bar{1}0)$-$Ni_{16}S_8$_2S_4SH, (c) $(10\bar{1}0)$-$Ni_{16}S_8$_4SH_4NiH, (d) $(10\bar{1}0)$-$Ni_{16}S_8$_6SH_2NiH, and (e) $(10\bar{1}0)$-$Ni_{16}S_8$_8SH hydrogenated surfaces. Blue, light blue, yellow, and white spheres are the Ni(1) nickel, Ni(2) nickel, sulfur, and hydrogen atoms, respectively. Coordinatively unsaturated Ni(2) nickel atoms are marked by a red asterisk.

Table 1 Bader charges (q) of the species adsorbed on the $(10\bar{1}0)$-$Ni_{16}S_8$_2S_4SH, and $(10\bar{1}0)$-$Ni_{16}S_8$_6SH_2NiH surfaces

Surface	q_S[a] (e)	q_{SH}[b] (e)	$q_{S(SH)}$[c] (e)	$q_{H(SH)}$[d] (e)	q_H[e] (e)
$(10\bar{1}0)$-$Ni_{16}S_8$_2S_4SH	−0.48	−0.26	−0.30	+0.04	—
$(10\bar{1}0)$-$Ni_{16}S_8$_6SH_2NiH	—	−0.26	−0.28	+0.02	−0.17
		−0.26	−0.31	+0.05	

[a] q_S charge of the adsorbed S atoms. [b] q_{SH} charge of the SH groups. [c] $q_{S(SH)}$ charge of the S atoms in the SH groups. [d] $q_{H(SH)}$ charge of the H atoms in the SH groups. [e] q_H charge of the H atoms in the NiH especies.

these plots, the blue regions represent electron density accumulation, and the red regions represent electron density depletion. For instance, the electron density accumulates on the adsorbed H atoms on the $(10\bar{1}0)$-$Ni_{16}S_8$_6SH_2NiH surface, which is consistent with a hydridic character. Additionally, the redistribution of electron density differs between the SH groups due to the local chemical environment that each SH group experiences in its immediate surroundings (Fig. 8b). Overall, these hydrogen species exhibit either proton or hydride character, depending on the electronegativity of their ligands (sulfur or metal).[18]

4. Conclusions

In this work, we carried out a comprehensive theoretical analysis of the structural and electronic properties of the active nickel and hydrogen species on the phosphosulfide phase formed on the (0001) and $(10\bar{1}0)$ surfaces under HDS reaction conditions.

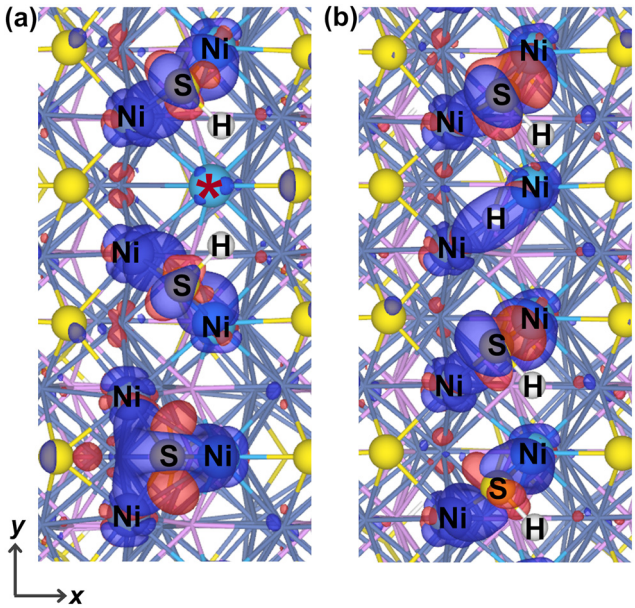

Fig. 8 EDD plots for the adsorption of the S, H, and SH species on the (a) $(10\bar{1}0)$-$Ni_{16}S_8$_2S_4SH and (b) $(10\bar{1}0)$-$Ni_{16}S_8$_6SH_2NiH surfaces. The blue and red regions represent the electron density gain and loss, respectively. The EDD was plotted using an isodensity level of 0.0035*e* Borh^{-3}. Blue, light blue, yellow, and white spheres are the Ni(1) nickel, Ni(2) nickel, sulfur, and hydrogen atoms, respectively.

The fully sulfided (0001) surface of Ni_2P, composed of Ni(1)-type atoms, closely resembles the (111) surface of the low-activity sulfide Ni_3S_2, suggesting that surfaces with spatially isolated Ni_3 ensembles that are not covered by sulfur are unlikely to be thermodynamically stable. Additionally, hydrogenated (0001) surfaces are not stable because, upon SH group formation, the sulfur atom binds to two of the three Ni(1) atoms within the Ni_3 site, leaving the third Ni(1) atom coordinatively unsaturated.

On the $(10\bar{1}0)$ surface, the SH groups were identified as the stable form of hydrogen adsorption. The $(10\bar{1}0)$-$Ni_{16}S_8$_2S_4SH surface, which has coordinatively unsaturated Ni(2) atoms surrounded by SH groups, was the most stable under HDS conditions. Hydrogen stabilization as a hydride, with H atoms adsorbed in a bridging position between the Ni(1) and Ni(2) atoms, only occurred under strong reducing conditions. Our results indicated that the formation of the proton-hydride pair may not occur under reaction conditions. Instead, only the proton species within SH groups are likely to play an active role in facilitating hydrogenation reactions on the nickel phosphosulfide overlayer formed on the Ni_2P catalyst. It should be emphasized that the surface structures identified in this work correspond to thermodynamically stable surfaces under equilibrium assumptions, rather than a unique description of the dynamic catalytic surface under reaction conditions.

Overall, these findings offer insight into processes occurring at the catalyst surface that may influence HYD selectivity at Ni(2) sites. Organosulfur species adsorbed at these sites may interact with protons from nearby SH groups, potentially forming hydrogenated intermediates and facilitating subsequent C–S bond hydrogenolysis.

Conflicts of interest

There are no conflicts to declare.

Data availability

The supporting data has been provided as part of the supplementary information (SI). Supplementary information is available. See DOI: https://doi.org/10.1039/d6cp00205f.

Acknowledgements

The DFT calculations were performed using computational resources from Laboratorio de Química Física y Catálisis Computacional (FONACIT Grant 20240PGP66) and Laboratorio de Fisicoquímica Teórica de Materiales (FONACIT Grant 2023PGP320).

References

1 K. K. Bando, T. Wada, T. Miyamoto, K. Miyazaki, S. Takakusagi, Y. Koike, Y. Inada, M. Nomura, A. Yamaguchi, T. Gott, S. Ted Oyama and K. Asakura, Combined in situ QXAFS and FTIR analysis of a Ni phosphide catalyst under hydrodesulfurization conditions, *J. Catal.*, 2012, **286**, 165–171.
2 L. Yang, X. Li, A. Wang, R. Prins, Y. Wang, Y. Chen and X. Duan, Hydrodesulfurization of 4,6-dimethyldibenzothiophene and its hydrogenated intermediates over bulk Ni_2P, *J. Catal.*, 2014, **317**, 144–152.
3 Y.-K. Lee and S. T. Oyama, Sulfur resistant nature of Ni_2P catalyst in deep hydrodesulfurization, *Appl. Catal., A*, 2017, **548**, 103–113.
4 P. J. Topalian, D. R. Liyanage, S. J. Danforth, A. I. d'Aquino, S. L. Brock and M. E. Bussell, Effect of Particle Size on the Deep HDS Properties of Ni_2P Catalysts, *J. Phys. Chem. C*, 2019, **123**, 25701–25711.
5 C. E. Miles, T. R. Carlson, B. J. Morgan, P. J. Topalian, J. R. Schare and M. E. Bussell, Hydrodesulfurization Properties of Nickel Phosphide on Boron-treated Alumina Supports, *ChemCatChem*, 2020, **12**, 4939–4950.
6 X. Zhou, X. Li, R. Prins, A. Wang, L. Wang, S. Liu and Q. Sheng, Desulfurization of 2-phenylcyclohexanethiol over transition-metal phosphides, *J. Catal.*, 2020, **383**, 331–342.
7 R. H. Bowker, G. H. Layan Savithra, B. A. Carrillo, K. G. Hubach, T. McDonald, S. L. Brock and M. E. Bussell, Effect of particle size on the sulfur resistance of nickel phosphide hydrodesulfurization catalysts, *J. Catal.*, 2023, **425**, 70–79.
8 S. Oyama, Effect of Phosphorus Content in Nickel Phosphide Catalysts Studied by XAFS and Other Techniques, *J. Catal.*, 2002, **210**, 207–217.
9 S. T. Oyama, X. Wang, Y.-K. Lee and W.-J. Chun, Active phase of Ni_2P/SiO_2 in hydroprocessing reactions, *J. Catal.*, 2004, **221**, 263–273.
10 Y. Shu, Y. Lee and S. Oyama, Structure-sensitivity of hydrodesulfurization of 4,6-dimethyldibenzothiophene over

silica-supported nickel phosphide catalysts, *J. Catal.*, 2005, **236**, 112–121.
11 T. Kawai, K. Bando, Y. Lee, S. Oyama, W. Chun and K. Asakura, EXAFS measurements of a working catalyst in the liquid phase: an in situ study of a Ni_2P hydrodesulfurization catalyst, *J. Catal.*, 2006, **241**, 20–24.
12 S. T. Oyama, T. Gott, K. Asakura, S. Takakusagi, K. Miyazaki, Y. Koike and K. K. Bando, In situ FTIR and XANES studies of thiophene hydrodesulfurization on Ni2P/MCM-41, *J. Catal.*, 2009, **268**, 209–222.
13 X. Duan, Y. Teng, A. Wang, V. Kogan, X. Li and Y. Wang, Role of sulfur in hydrotreating catalysis over nickel phosphide, *J. Catal.*, 2009, **261**, 232–240.
14 X. Li, Z. Sun, A. Wang, Y. Wang, X. Duan and Y. Chen, XAS study of Ni_2P/MCM-41 passivated by O_2/He and H_2S/H_2, *Catal. Commun.*, 2014, **43**, 21–24.
15 S. Tian, X. Li, A. Wang, R. Prins, Y. Chen and Y. Hu, Facile Preparation of Ni_2P with a Sulfur-Containing Surface Layer by Low-Temperature Reduction of $Ni_2P_2S_6$, *Angew. Chem., Int. Ed.*, 2016, **55**, 4030–4034.
16 M. He, T. Li, X. Li, A. Wang, Q. Sheng, S. Shang and Z. Yu, Preparation of Ni_2P with a Surface Nickel Phosphosulfide Layer by Reduction of Mixtures of $Na_4P_2S_6$ and $NiCl_2$, *ChemCatChem*, 2024, e202400823.
17 S. Rangarajan and M. Mavrikakis, DFT Insights into the Competitive Adsorption of Sulfur- and Nitrogen-Containing Compounds and Hydrocarbons on Co-Promoted Molybdenum Sulfide Catalysts, *ACS Catal.*, 2016, **6**, 2904–2917.
18 H. Cai, R. Schimmenti, H. Nie, M. Mavrikakis and Y.-H. C. Chin, Mechanistic Role of the Proton–Hydride Pair in Heteroarene Catalytic Hydrogenation, *ACS Catal.*, 2019, **9**, 9418–9437.
19 N. Y. Topsoe and H. Topsoe, FTIR Studies of Mo/Al2O3-Based Catalysts, *J. Catal.*, 1993, **139**, 641–651.
20 G. Berhault, M. Lacroix, M. Breysse, F. Maugé, J.-C. Lavalley, H. Nie and L. Qu, Characterization of Acidic Sites of Silica-Supported Transition Metal Sulfides by Pyridine and 2,6 Dimethylpyridine Adsorption: Relation to Activity in CH_3SH Condensation, *J. Catal.*, 1998, **178**, 555–565.
21 S. Oyama and Y. Lee, The active site of nickel phosphide catalysts for the hydrodesulfurization of 4,6-DMDBT, *J. Catal.*, 2008, **258**, 393–400.
22 A. Nelson, M. Sun and A. Junaid, On the structure and composition of the phosphosulfide overlayer on Ni_2P at hydrotreating conditions, *J. Catal.*, 2006, **241**, 180–188.
23 L. L. D. Thi, P. N. K. Tuyen and T. Y. Vu, Flower-like S-doped-Ni_2P mesoporous nanosheet-derived self-standing electrocatalytic electrode for boosting hydrogen evolution, *Nanotechnology*, 2020, **31**, 465401.
24 X. Wang, Q. Hu, G. Li, S. Wei, H. Yang and C. He, Regulation of the adsorption sites of Ni_2P by Ru and S co-doping for ultra-efficient alkaline hydrogen evolution, *J. Mater. Chem. A*, 2021, **9**, 15648–15653.
25 Y. Wu, X. Chen, L. Su, Q. Wang and S. Ren, A sulfur-doped Ni_2P electrocatalyst for the hydrogen evolution reaction, *New J. Chem.*, 2022, **46**, 7675–7681.
26 M. Šarić, P. G. Moses and J. Rossmeisl, Relation between Hydrogen Evolution and Hydrodesulfurization Catalysis, *ChemCatChem*, 2016, **8**, 3334–3337.
27 A. J. McCue and J. A. Anderson, Sulfur as a catalyst promoter or selectivity modifier in heterogeneous catalysis, *Catal. Sci. Technol.*, 2014, **4**, 272–294.
28 G. Kresse and J. Hafner, *Ab initio* molecular dynamics for liquid metals, *Phys. Rev. B: Condens. Matter Mater. Phys.*, 1993, **47**, 558–561.
29 G. Kresse and J. Furthmüller, Efficient iterative schemes for *ab initio* total-energy calculations using a plane-wave basis set, *Phys. Rev. B: Condens. Matter Mater. Phys.*, 1996, **54**, 11169–11186.
30 J. P. Perdew, K. Burke and M. Ernzerhof, Generalized Gradient Approximation Made Simple, *Phys. Rev. Lett.*, 1996, **77**, 3865–3868.
31 G. Kresse and D. Joubert, From ultrasoft pseudopotentials to the projector augmented-wave method, *Phys. Rev. B: Condens. Matter Mater. Phys.*, 1999, **59**, 1758–1775.
32 S. Grimme, J. Antony, S. Ehrlich and H. Krieg, A consistent and accurate *ab initio* parametrization of density functional dispersion correction (DFT-D) for the 94 elements H-Pu, *J. Chem. Phys.*, 2010, **132**, 154104.
33 W. Hujo and S. Grimme, Comparison of the performance of dispersion-corrected density functional theory for weak hydrogen bonds, *Phys. Chem. Chem. Phys.*, 2011, **13**, 13942.
34 J. P. P. Ramalho, J. R. B. Gomes and F. Illas, Accounting for van der Waals interactions between adsorbates and surfaces in density functional theory based calculations: selected examples, *RSC Adv.*, 2013, **3**, 13085.
35 S. Banerjee, A. Kakekhani, R. B. Wexler and A. M. Rappe, Relationship between the Surface Reconstruction of Nickel Phosphides and Their Activity toward the Hydrogen Evolution Reaction, *ACS Catal.*, 2023, **13**, 4611–4621.
36 S. Rundqvist, M. Yhland, R. Dahlbom, J. Sjövall, O. Theander and H. Flood, X-Ray Investigations of Mn_3P, Mn_2P, and Ni_2P, *Acta Chem. Scand.*, 1962, **16**, 992–998.
37 M. E. Fleet, The crystal structure of heazlewoodite, and metallic bonds in sulfide minerals, *Am. Mineral.*, 1977, **62**, 341–345.
38 R. F. W. Bader, A quantum theory of molecular structure and its applications, *Chem. Rev.*, 1991, **91**, 893–928.
39 K. Momma and F. Izumi, *VESTA3* for three-dimensional visualization of crystal, volumetric and morphology data, *J. Appl. Crystallogr.*, 2011, **44**, 1272–1276.
40 W. Papawassiliou, J. P. Carvalho, N. Panopoulos, Y. Al Wahedi, V. K. S. Wadi, X. Lu, K. Polychronopoulou, J. B. Lee, S. Lee, C. Y. Kim, H. J. Kim, M. Katsiotis, V. Tzitzios, M. Karagianni, M. Fardis, G. Papavassiliou and A. J. Pell, Crystal and electronic facet analysis of ultrafine Ni_2P particles by solid-state NMR nanocrystallography, *Nat. Commun.*, 2021, **12**, 4334.
41 J. He, Á. Morales-García, O. Bludský and P. Nachtigall, The surface stability and equilibrium crystal morphology of Ni_2P nanoparticles and nanowires from an ab initio atomistic thermodynamic approach, *CrystEngComm*, 2016, **18**, 3808–3818.
42 A. B. Vidal, J. L. Peña-Mena, O. Hurtado-Aular, R. Añez and A. Sierraalta, Unraveling the Structure and Surface Chemistry of the Phosphosulfide Phase Formed on Ni_2P under

Hydrodesulfurization Reaction Conditions: A DFT Study, *J. Phys. Chem. C*, 2022, **126**, 14187–14200.
43 A. Aguinaga, M. Montes, P. Malet, M. J. Capitán, I. Carrizosa and J. A. Odriozola, Extended X-ray absorption fine structure study of sulphur poisoned Ni/SiO_2 catalysts, *Appl. Catal., A*, 1994, **110**, 197–205.
44 J. R. Rostrup-Nielsen, J. Sehested and J. K. Nørskov, *Advances in Catalysis*, Elsevier, 2002, vol. 47, pp. 65–139.
45 X. Chen, J. Jiang, F. Yan, K. Li, S. Tian, Y. Gao and H. Zhou, Dry Reforming of Model Biogas on a Ni/SiO_2 Catalyst: Overall Performance and Mechanisms of Sulfur Poisoning and Regeneration, *ACS Sustainable Chem. Eng.*, 2017, **5**, 10248–10257.
46 R. Prins and M. E. Bussell, Metal Phosphides: Preparation, Characterization and Catalytic Reactivity, *Catal. Lett.*, 2012, **142**, 1413–1436.
47 T. Pecoraro and R. Chianelli, Hydrodesulfurization catalysis by transition metal sulfides, *J. Catal.*, 1981, **67**, 430–445.
48 J. Quartararo, S. Mignard and S. Kasztelan, Hydrodesulfurization and hydrogenation activities of alumina-supported transition metal sulfides, *J. Catal.*, 2000, **192**, 307–315.
49 G. Kishan, L. Coulier, V. H. J. de Beer, J. A. R. van Veen and J. W. Niemantsverdriet, Sulfidation and Thiophene Hydrodesulfurization Activity of Nickel Tungsten Sulfide Model Catalysts, Prepared without and with Chelating Agents, *J. Catal.*, 2000, **196**, 180–189.
50 Y. Lee and S. Oyama, Bifunctional nature of a SiO_2-supported Ni_2P catalyst for hydrotreating: EXAFS and FTIR studies, *J. Catal.*, 2006, **239**, 376–389.
51 R. R. Chianelli, T. A. Pecoraro, T. R. Halbert, W. H. Pan and E. I. Stiefel, Transition metal sulfide catalysis: relation of the synergic systems to the periodic trends in hydrodesulfurization, *J. Catal.*, 1984, **86**, 226–230.
52 Y. Aray, D. Vega, J. Rodriguez, A. B. Vidal, M. Elena Grillo and S. Coll, First-Principles Study of Low Miller Index Ni_3S_2 Surfaces in Hydrotreating Conditions, *J. Phys. Chem. B*, 2009, **113**, 3058–3070.
53 R. Khare, R. Weindl, A. Jentys, K. Reuter, H. Shi and J. A. Lercher, Di- and Tetrameric Molybdenum Sulfide Clusters Activate and Stabilize Dihydrogen as Hydrides, *JACS Au*, 2022, **2**, 613–622.